Mon. Not. R. Astron. Soc. **000**, 1–11 (2010) Printed 26 April 2010 (MN LATEX style file v2.2)

A Synthetic 21-cm Galactic Plane Survey of an SPH Galaxy Simulation

Kevin A. Douglas[1],⋆ David M. Acreman[1], Clare L. Dobbs[1,2,3], and Christopher M. Brunt[1]

[1] *School of Physics, University of Exeter, Stocker Road, Exeter, UK EX4 4QL*
[2] *Max-Planck-Institut für extraterrestrische Physik, Giessenbachstraße, D-85748 Garching, Germany*
[3] *Universitats-Sternwarte München, Scheinerstraße 1, D-81679 München, Germany*

26 April 2010

ABSTRACT

We have created synthetic neutral hydrogen (H I) Galactic Plane Survey data cubes covering $90° \leqslant \ell \leqslant 180°$, using a model spiral galaxy from SPH simulations and the radiative transfer code TORUS. The density, temperature and other physical parameters are fed from the SPH simulation into TORUS, where the H I emissivity and opacity are calculated before the 21-cm line emission profile is determined. Our main focus is the observation of Outer Galaxy 'Perseus Arm' H I, with a view to tracing atomic gas as it encounters shock motions as it enters a spiral arm interface, an early step in the formation of molecular clouds. The observation of H I self-absorption features at these shock sites (in both real observations and our synthetic data) allows us to investigate further the connection between cold atomic gas and the onset of molecular cloud formation.

Key words: surveys, ISM: strucutre, atoms

1 INTRODUCTION

The formation of molecular clouds out of cold, dense atomic gas is a key process in the cyclic evolution of the interstellar medium. Above column densities of $N_H \approx 10^{20}$ cm^{-2}, atomic hydrogen gas transitions to molecular H_2, a critical step towards the formation of stellar systems (Dixon et al. 1998). For the molecular fraction of the gas to remain stable depends largely on the ability of the molecular gas to self-shield against dissociating photons from the local radiation field. Moreover, the importance of dust grains in H_2 formation requires their presence in these transition interfaces.

The 21-cm neutral hydrogen line is the main tracer of interstellar structure. The ubiquitous nature of atomic hydrogen in the Galaxy was demonstrated in early surveys (Oort et al. 1958), and more recent surveys imaging the H I distribution at moderately high resolution (parsec scales at distances of kpc) have steadily improved upon that view. Almost all of the H I in the Galaxy's disc has been sampled by the International Galactic Plane Survey (IGPS; Stil et al. (2006); McClure-Griffiths et al. (2005); Taylor et al. (2003)). Beyond the Galactic Plane, all-sky mapping efforts of the Southern (GASS; McClure-Griffiths et al. (2009)) and Northern skies (EBHIS; Kerp et al. (2009)) have improved vastly on the previous generation's all-sky H I maps. Galactic 21 cm surveys at Arecibo with its ALFA instrument (Peek et al. 2008, 2009; van Loon et al. 2009; Putman et al. 2009) are revealing H I structures in our Galactic neighbourhood with unprecedented sensitivity.

Observational evidence of the interface between atomic and molecular gas relies on a good H_2 tracer. The $J = 1 - 0$ rotational transition of CO is the most common surrogate of molecular hydrogen, yet there are conditions under which its efficacy as a reliable H_2 tracer is undermined (Douglas & Taylor 2007; Klaassen et al. 2005; Dobbs & Bonnell 2007; Pelupessy & Papadopoulos 2009). For example, in photon-dominated regions, the CO molecule is largely dissociated, while H_2 self-shielding allows for a significant amount of molecular gas to remain. In very cold, dense molecular cores, CO will freeze onto dust grains along with other larger molecules, and so the H_2 content in such cores would be underestimated by traditional CO observations. In addition to the above scenarios, which assume a molecular cloud has already formed, a newly forming molecular cloud must have an epoch wherein a significant quantity of H_2 has formed before an appreciable (detectable) amount of CO has been reached (Bergin et al. 2004), and so the evolution of protostellar objects may be already underway in molecular clouds before the onset of critical CO densities. OH is another molecule which has been used to probe the H-H_2 transition region, with some suc-

⋆ email: douglas@astro.ex.ac.uk

cess (Magnani & Siskind 1990; Wannier et al. 1993). Neutral and ionised carbon atoms also have potential to be good tracers of diffuse, pre-CO molecular gas (Oka et al. 2005).

In order for appreciable H_2 to form from a largely atomic hydrogen reservoir, the gas must be cooled to temperatures on the order of 20 K, among other favourable conditions (sufficient number densities, H_2 formation sites). Models of gas flowing into the Perseus spiral arm (Roberts 1972) predict compression of the H I gas at the interface of a "shock ridge." Though his model was isothermal, such conditions are favourable for strong cooling of H I, leading to self-absorption of 21-cm emission, and possibly enhanced H_2 production. Hence H I self-absorption (HISA) observations may help to trace the earliest stages of molecular cloud formation, in regions where CO is not a workable tracer for molecular hydrogen. Widespread HISA has been observed in the Outer Galaxy (Gibson et al. 2005), and its association with CO is anything but straightforward. HISA and CO emission are often found to be coincident spatially and at the same radial velocities, but the correspondence is complicated. There are regions where only one is present, which may indicate differences in the evolutionary state of these clouds. Studies of HISA and OH emission have found the OH emission to be more localised to the HISA (Kavars 2006; Li & Goldsmith 2003), compared to CO. As an extra complication, the detection of HISA requires background H I emission at the same velocity as the absorbing gas, which may not be available along many lines of sight.

In addition to analytical models, computational efforts have investigated this scenario in detail. Dobbs et al. (2008) performed galaxy-scale SPH simulations that trace the dynamics of interstellar clouds as they encounter shocks in spiral arms. To enhance resolution in the spiral arms, their model traces only those SPH particles in a galactocentric annulus between $R_g = 5$ kpc out to $R_g = 10$ kpc. In addition to strong cooling of the atomic gas, molecular hydrogen forms in the vicinity of the shocks. Smaller clouds aggregrate into larger ones within the spiral shock, where the molecular fraction is $\geqslant 0.5$. As the clumps leave the spiral arm they are sheared into smaller spurs and lose most of their molecular gas.

The link between these models and observations can be strengthened by deriving predicted observables directly from the simulations. We do not observe densities, temperatures and pressures of clouds directly—rather, we rely on spectral line and continuum processes to deliver photons containing the valuable information, from which we infer the state of the object under study. As radiative transfer is a guiding principle for this propagation of information, we endeavour to simulate the creation of observable photons via radiative transfer, within the modelled physical representation of the ISM in our Galaxy. Gibson (2006) demonstrated the production of HISA by spiral shocks with a two-dimensional, purely atomic (cold and warm H I) radiative transfer model.

In this paper we present results from generating synthetic H I spectral line datacubes from a multiphase numerical galaxy calculation. The aforementioned SPH calculation by Dobbs et al. (2008) is used as a basis to create a synthetic Galactic Plane survey, fashioned after the H I data products created for the IGPS. Simulating such surveys requires the "observer" to be placed at an appropriate position inside the simulated Galaxy. Such challenges are accomplished using TORUS, an Adaptive Mesh Refinement (AMR) code which is capable of performing radiative transfer calculations to produce synthetic spectra (Harries 2000). Moreover, the added flexibility of operating on a numerical model enables us to use the same code to observe the Galaxy from multiple positions, as well as to emulate extragalactic H I observations (Acreman et al. 2010).

This paper is organised in the following way. Section 2 reviews the method used to create our synthetic Galactic Plane Survey, and the data cubes produced are described in section 3. In section 4 we discuss the use of HISA profiles as a diagnostic of early molecular cloud formation. In section 5 we compare briefly our synthetic data to observational H I profiles of the Milky Way, setting the basis for a discussion of how future refinements to our investigation, such as the incorporation of feedback mechanisms, will bring closer agreement between the synthetic and observed H I distributions.

2 NUMERICAL WORK: SPH SIMULATIONS AND TORUS

The method for creating synthetic H I cubes has been outlined previously in Acreman et al. (2010), hereafter called Paper I. We briefly summarise the main points here.

An SPH spiral galaxy calculation is fed into TORUS, wherein the particle representation of the gas is transformed into a gridded representation, aided by AMR to provide the best resolution in regions of highest density. Next, radiative transfer calculations and ray tracing algorithms produce synthetic spectra for lines of sight chosen from an arbitrary observing position. The intensities determined by the radiative transfer and ray tracing are converted to a brightness temperature T_b, using the Rayleigh-Jeans approximation. In Paper I we demonstrated this method by simulating 21-cm H I observations of nearby spiral galaxies, assigning the SPH galaxies orientations and systemic velocities matching M31 and M33.

Moreover, the observer can be placed within the galaxy, allowing for the simulation of *Galactic* H I observations to be performed. In such cases, some adaptations of TORUS algorithms must be made. The AMR grid is generated at a much finer resolution than that used in Paper I, in order to provide better resolution for structure close to the observer. The maximum H I mass per cell for the AMR grids used in this paper is 2.5×10^{34} g (12.6 $M_\odot$), which is a factor of 100 smaller than that used in paper I. In order to cope with the increased number of cells in the AMR grid, the domain of the grid is restricted to exclude regions of the galaxy which are not relevant to the cube being calculated. A different AMR grid is used for generating each data cube but they typically comprise 6×10^6 unique voxels.

Also, while the same ray-tracing method is used for both the external and internal views, its execution must be handled differently if we are to consider multiple lines of sight. For the external case the rays are essentially parallel, whereas in the internal case there is an obvious angular dependence to the observations. Additionally, by reversing the direction of ray trace, relative to that employed in Paper I (i.e. back to front rather than front to back), we are able to calculate the contribution of each cell of the AMR grid

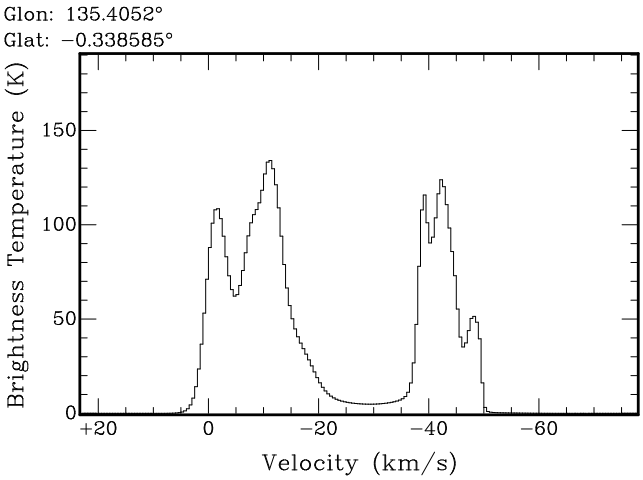

Figure 1. A synthetic H I spectrum measured from within the model galaxy, toward a position near Galactic coordinates $\ell = 135.5°, b = -0.3°$.

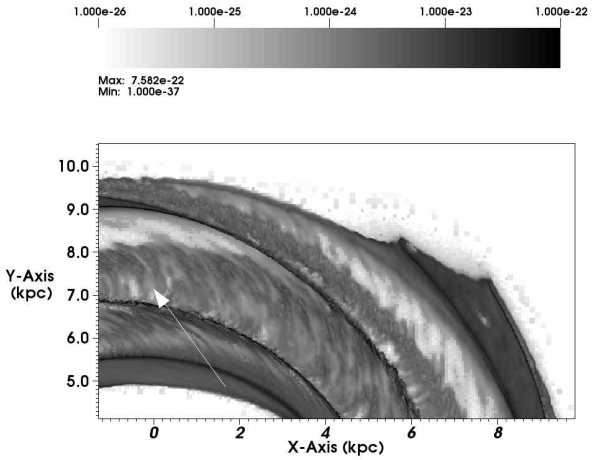

Figure 2. A midplane density slice of the simulated Galaxy gridded by TORUS, and showing the position of our "observer" for the synthetic Galactic Plane Survey.

to either the emission or absorption in a given data cube pixel. This feature is used to decompose spectral features into separate emission and absorption components, as part of our investigation of HISA in spiral arms. These differences are critical when we extend the creation of single spectra to making fully three-dimensional datacubes of simulated H I emission. The cubes are discussed in the next section.

Figure 1 shows an H I spectrum measured from a position within the SPH galaxy, corresponding roughly to the Earth's position in our Galaxy, toward a direction corresponding to Galactic longitude $\ell \approx 135.5°$ and latitude $b \approx -0.3°$. We see "local" spiral arm gas in a radial velocity range $-20 < v_r < 0$ km s^{-1}, and an outer arm beyond $v_r \approx -38$ km s^{-1}. The outer arm shows some evidence of H I absorption, with a narrow dip in T_b appearing near $v_r = -41$ km s^{-1}. This HISA signature is common in synthetic spectra all across our region of interest. Since HISA is a main focus of our investigation into molecular cloud formation, the TORUS code was modified so that in addition to total brightness temperature cubes, we create separate datacubes where only positive or negative intensity contributions (dI) for a given grid cell are mapped.

For this paper, the simulated galaxy has reached a time of 250 Myr. At this age the distribution of gas in different phases, and the fraction of molecular gas, have reached a roughly steady state. While tracing the evolution of specific ISM structures using many timesteps from an SPH simulation is the subject of future investigations, the present work concentrates on deriving H I properties from a single epoch, as is the case with most Galactic radio observations. As mentioned previously, the models are restricted to Galactocentric radii of 5 to 10 kpc. For this reason it is reasonable to aim to reproduce observations of the Outer Galaxy, toward its Anticenter ($\ell = 180°$). In this paper, we survey the entire second quadrant of our SPH galaxy, covering longitudes between $\ell = 90°$ and $\ell = 180°$.

Table 1. Second Quadrant Mosaic Regions

Region Name	$\ell_{central}$ (°)
ABC	99.0
DEF	117.0
GHI	135.0
JKL	153.0
MNO	171.0

3 SYNTHETIC DATACUBES OF H I BRIGHTNESS

For the Galactic point of view, we construct $T_b(\ell, b, v_r)$ cubes with angular coordinates corresponding to "Galactic" coordinates from the position of the observer. This position is chosen to be in the midplane, 2.2×10^{22} cm (7.13 kpc) from the galaxy's center, as illustrated in figure 2. This choice corresponds to a position in an interarm "spur" of H I, similar to the Orion Spur of our Milky Way.

3.1 Channel Maps

A total of fifteen cubes of angular dimension $6.08° \times 6.08°$ are produced to cover the entire Second Quadrant, with a small amount of overlap between adjacent fields for mosaicking purposes. With an image scale of $0.5'$ per pixel, each channel map produced by TORUS measures 732^2 pixels. Our spectral range covers radial velocities from +30 km s^{-1} to −120 km s^{-1} sampled at 0.5 km s^{-1}, resulting in 300 channels for each cube produced by TORUS.

For ease of visualisation, the fifteen cubes are combined into five mosaics, summarised in table 1. Each mosaic region therefore covers just over 18° of Galactic longitude, centered on the value of $\ell_{central}$ given in the table. For il-

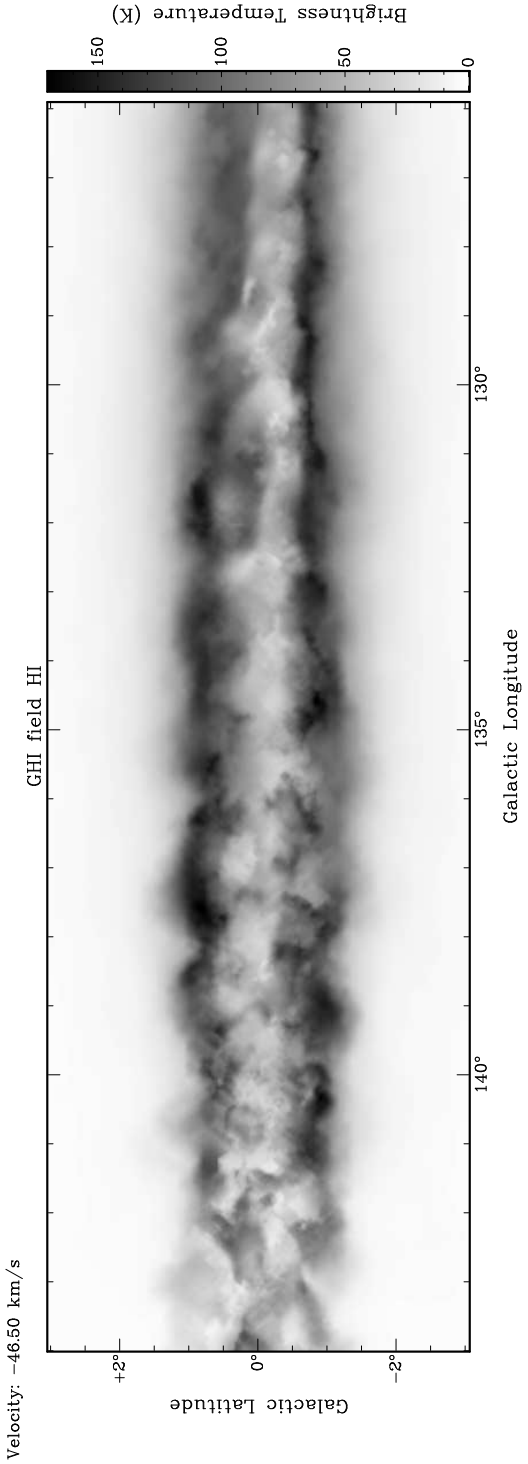

Figure 3. Synthetic Perseus Arm (SPA) gas near $v_r = -45$ km/s for the GHI region ($126° \leqslant \ell \leqslant 144°$).

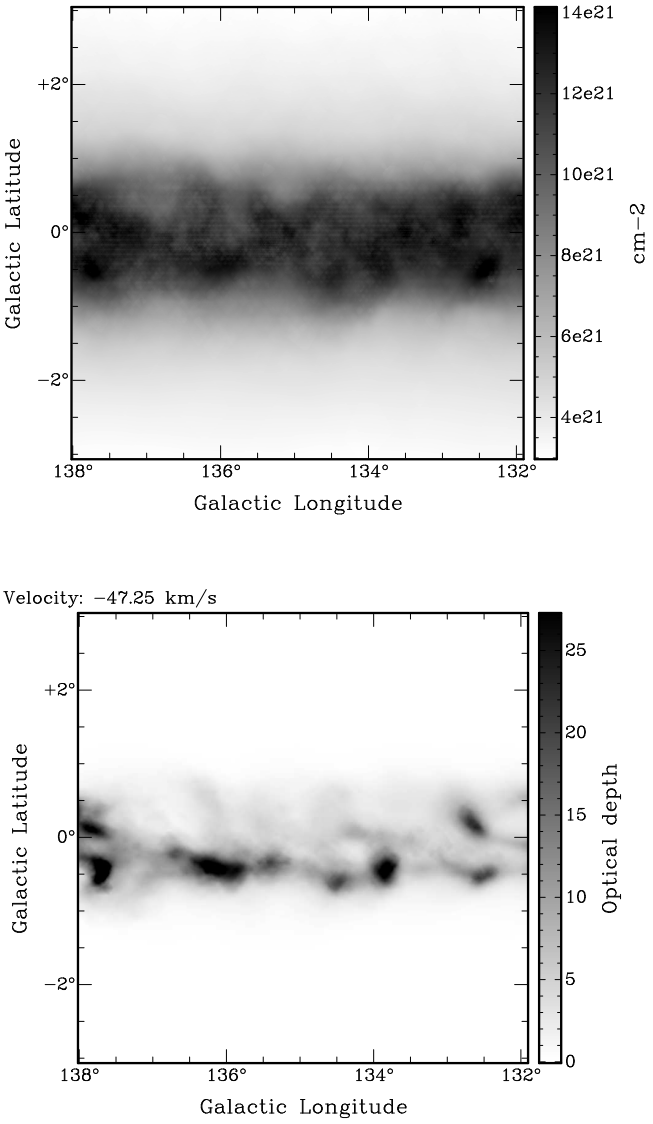

Figure 4. Column density map (top) and optical depth channel map (bottom) for the SPA cube centered on $\ell = 135°$, $b = 0°$.

lustrative purposes we show a channel map from the central mosaic, region GHI, in Figure 3. This channel map shows H I gas near $v_r = -45$ km s^{-1}, as our aim is to study HISA produced in spiral arm gas with radial velocities corresponding to Perseus Arm gas (we will refer to the simulation's "Perseus Arm" as the "SPA").

A common feature seen in our SPA channel maps is that the brightest H I emission appears not in the central midplane ($b = 0°$) of the spiral arm, where the densities are greatest, but in ridges at approximately $\pm 1°$ above and below the midplane. From the known distribution of gas column density in the original SPH simulations, the expected H I distribution assuming optical thinness would not have predicted such a pattern for maximal brightness temperatures. Rather, this is an absorption effect arising from a highly dense and cold central ($|b| < 0.5°$) midplane. As figure 4 (top panel) demonstrates for the cube toward $\ell = 135°$, the synthetic H I clouds occupy the plane quite randomly, mostly within $|b| < 1°$. With an increase in column density, an increased optical depth τ of H I follows naturally. As a result, the midplane of the SPA is largely optically thick. With TORUS we can construct cubes of $\tau(\ell, b, v_r)$ in addition to T_b, and we show an example channel map of τ in the SPA for

the same region in the lower panel of figure 4. Individual H I clouds exhibit optical depth values $\tau \geqslant 15$, and thus the H I gas nearer the midplane absorbs much more strongly, and the brightness temperatures are diminished by the combination of high opacity and colder temperatures. The optical depths above $|b| = 0.5^\circ$ are considerably lower, and so we observe emission rather than absorption.

Another observed (and related) consequence of the overdense, high-τ SPA plane is that the amount of absorption seen in the SPA greatly exceeds the HISA distribution found in the Perseus Arm of the Milky Way. While this level of self-absorption is greater than what is expected from Galactic studies (Gibson et al. 2005; Goldsmith et al. 2007), the exaggerated contrast between emission and absorption in the SPH galaxy allows us to investigate the HISA phenomenon in a more "controlled" interstellar environment. As mentioned above, we make separate cubes which track pixels where brightness temperature increases or decreases along the line of sight, as a means of tracing regions where self-absorption occurs.

Figure 5 shows positive-only and negative-only spectra for the line of sight total-T_b spectrum shown in figure 1, and channel maps for region GHI at the same radial velocity as shown in figure 3. The negative-only spectra and channel maps are very useful in isolating HISA features in our synthetic survey; the majority of negative-T_b pixels lie in the plane at radial velocities corresponding to the SPA. We will return to our analysis of HISA features in the next section.

3.2 Position-Velocity Views

In figure 6 we show the Galactic view toward $\ell = 135^\circ$ again (region GHI), with an $\ell - v_r$ cut along $b = 0^\circ$. The main feature to be elucidated is the separation of local ($v_r \approx 0$) H I from gas at synthetic Perseus Arm (SPA) velocities, near -35 to -55 km/s. The local gas has little discernable structure in our synthetic cube, as its proximity to the observer position means the gas has a very large angular extent. As is the case with our Galaxy, the mean radial velocity of the SPA becomes less negative toward higher longitudes, and blends with the local gas toward the Anticenter, a projection effect based on Galactic rotation. Toward lower longitudes, the SPA spans a larger range of radial velocities.

Beyond the SPA, there is no outer spiral arm across the Second Quadrant, until the appearance of terminating spiral arms from spiral structure originating toward the Inner Galaxy. Across the Second Quadrant there are discrete clouds, containing high fractions of molecular gas in many instances, which exit the outer edge of the SPA, but these clouds mostly share radial velocities with H I gas within the SPA.

As we move away from the midplane in the longitude-velocity projection, the SPA shows bright H I emission out to $|b| \approx 1.3^\circ$, after which its intensity drops sharply as one moves further from the midplane. This effect is shown toward $\ell = 135^\circ$ in figure 7. With a distance to the SPA of 2 kpc (at its closest), this vertical distribution suggests that most of the H I is confined to within ~ 100 pc of the midplane.

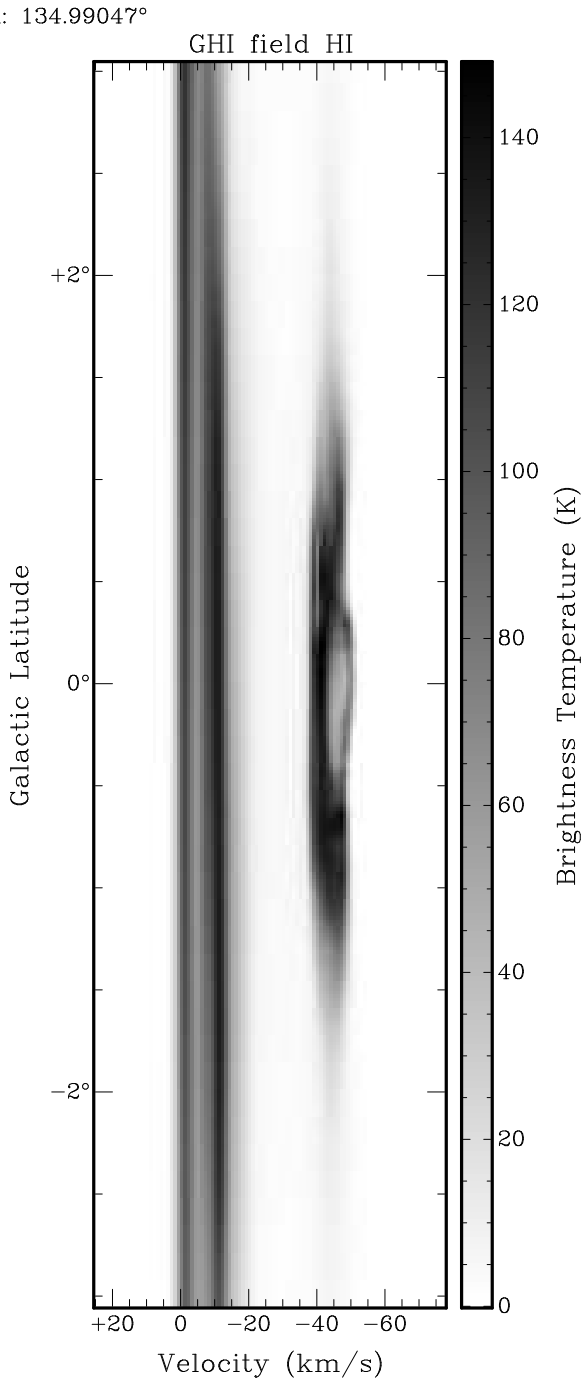

Figure 7. Latitude-velocity slice of synthetic H I toward a Galactic longitude of $\ell = 135^\circ$. The SPA H I emission is mostly confined to within 1 degree of the midplane.

4 HISA AND SPIRAL SHOCKS

In our Galaxy, HISA features tend to outline individual clouds or complexes of cold H I (Gibson et al. 2005; Kavars et al. 2005; McClure-Griffiths et al. 2006). By contrast, our synthetic data show large bands of HISA that subtend much larger angular extents. While unrealistic, this large abundance of HISA gives us many sightlines to test its origin.

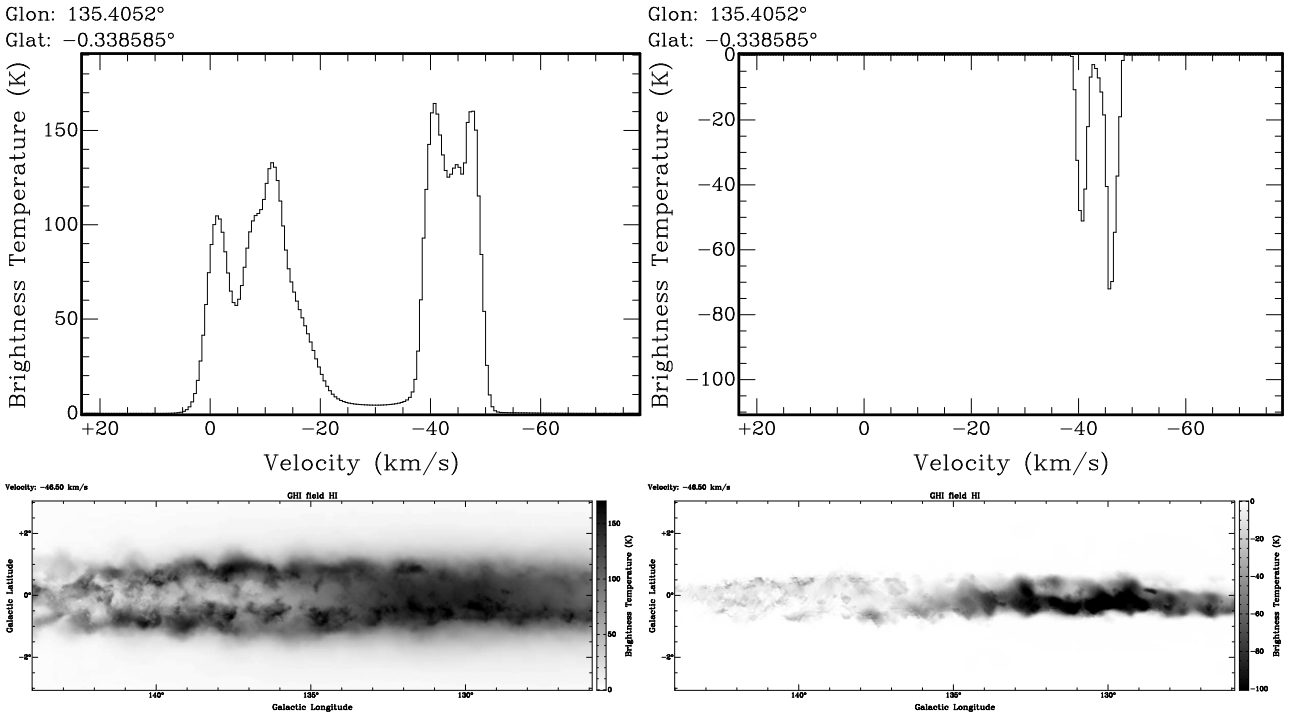

Figure 5. Synthetic H I emission-only (left) and absorption-only (right) spectra and channel maps. The spectra are for the same line of sight as in figure 1, but with the positive and negative T_b contributions separated. The channel maps show the same, for all of region GHI (see figure 3).

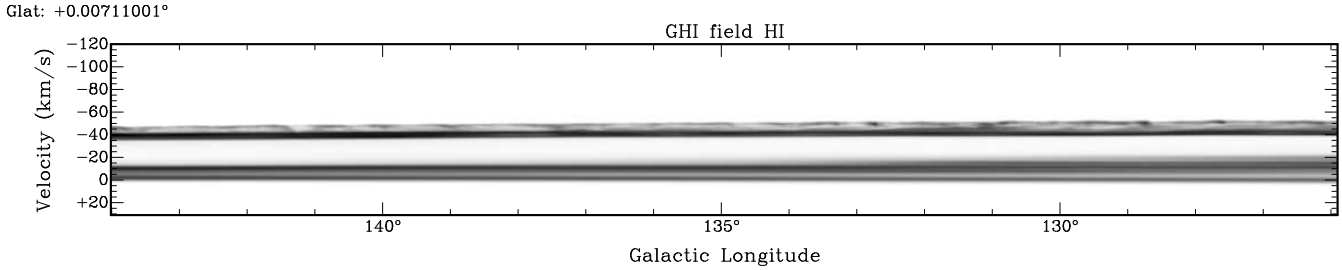

Figure 6. Longitude-velocity diagram of simulated H I emission near $\ell = 135°, b = 0°$ for the Galactic synthetic observation. Local and Perseus Arm gas are well separated.

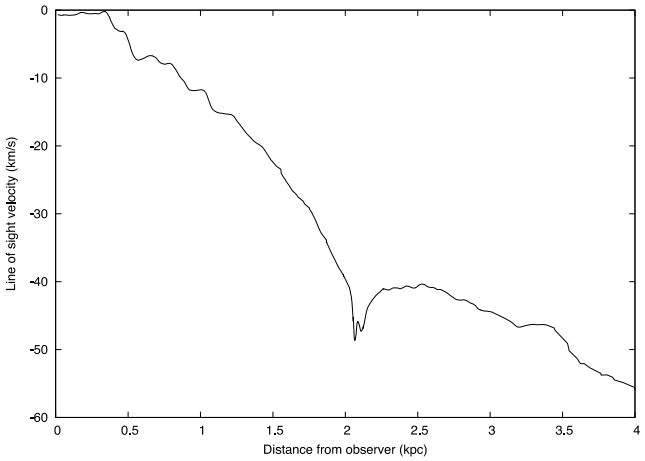

Figure 8. Radial velocity of the gas plotted against distance, for $\ell \approx 130.5°$, $b \approx -0.38°$ in the simulated galaxy.

The scenario described by Roberts (1972) for shock-induced compression of H I (as evidenced via HISA) can be tested directly with our simulations. Figure 8 shows a plot of the radial velocity for gas along a line of sight toward a position in region GHI, with $\ell \approx 130.5°$ and $b \approx -0.38°$. Between the observer and a distance of about 2 kpc, the radial velocity of the gas decreases steadily as a result of the gas moving with the rotation of the galaxy. Then, at a distance of 2 kpc, the radial velocity undergoes a sharp decrease from about -40 km s^{-1} down to a local minimum of approximately -50 km s^{-1}. The radial velocity remains in this range as we continue to move away from the observer, until about 2.2 kpc, where it slowly rises to -40 km s^{-1} and levels off for about half a kiloparsec, before again decreasing very gradually beyond 2.7 kpc.

The dip near 2 kpc corresponds to the near edge of the SPA, and we interpret this sharp decline in radial velocity as the result of the H I gas experiencing a shock in the spiral arm, where it loses much of its line of sight velocity as

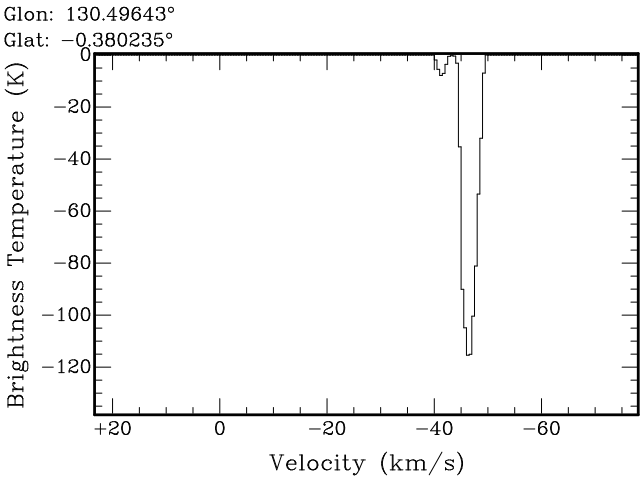

Figure 9. The HISA profile (ie. negative-T_b-only spectrum) toward the position described in figure 8. The radial velocities where HISA occurs are between −40 and −50 km s^{-1}, exactly where it would be expected from figure 8.

it begins to travel along the spiral arm edge. The gas cools during this process, and so the hydrogen at 2 kpc will absorb the H I emission from the gas behind it with the same radial velocity, resulting in strong HISA present in the spectrum between −40 and −50 km s^{-1}. Indeed we show in figure 9 that this is the precise radial velocity range where HISA is prevalent at this same position in the datacube. This confirmation of the Roberts (1972) scenario for H I shocks, in a region where molecular clouds are also formed in the model, shows the value of HISA as a tracer of the atomic-molecular interface of the ISM.

In figure 10 we zoom in to distances corresponding to the SPA, for the same line of sight as figure 8. While this sightline shows appreciable HISA, there is nothing extraordinary about it compared to other regions across the SPA. It is a fair representation of the type of H I profiles observed across the midplane of our synthetic survey. As shown in the top left panel, the density of neutral hydrogen rises by two orders of magnitude between 2.0 and 2.1 kpc from the observer, as the spiral arm boundary is crossed. While a single-fluid ($\gamma = \frac{5}{3}$) adiabatic shock would result in at most a factor of four density enhancement, such conditions would not constrain a strongly cooling shock, which describes the present scenario. Indeed, a corresponding drop in gas temperature is shown in the top right panel, as the gas cools strongly from values of $\sim$ 3000 K down to less than 100 K. In the lower left figure, we plot the H_2 fraction, by mass, of the total gas. The first peak, between 2.0 and 2.1 kpc, is interpreted as newly formed H_2 that has been formed in the vicinity of the shock at that site in the SPA. The other two high-H_2 areas beyond the shock, near 2.25 and 2.6 kpc, would be (giant) molecular clouds that were formed upstream by the same shock mechanism, at higher longitude, and which are moving through the SPA. In the absence of feedback in our simulation, these clouds may be larger than expected, and longer-lived. The outer edge of the SPA is less easy to define than the inner edge, given that there is no sharp outer boundary, but across much of the SPA, the density begins to decrease toward interarm values approximately 0.7 to 0.8 kpc behind the inner boundary.

The effect of these density and temperature variations on the observed H I profile can be informed by the lower right panel of figure 10, which shows the intensity contribution dI per unit of column density as a function of distance. HISA (negative dI) appears to be produced behind the shock, once the temperature has dropped to below 100 K, and where the H I density is above 10^{-23} g cm^{-3}. At the front of the shock there is a narrow region where emission is produced rather than absorption, because the gas is still quite warm, yet the H I density is already increasing rapidly. Such conditions are favourable for the onset of H_2 production, which depends strongly on density as well as weakly on temperature (Bergin et al. 2004). Still, this shows that within the region where the gas velocity is strongly influenced by the spiral arm shock, both emission and absorption from H I atoms are possible. Yet we can constrain the occurrence of HISA to cold, dense regions which also contain molecular gas. The temperature appears to remain at values around 100 K out to a distance of $\sim$ 2.65 kpc, after which it begins to rise and the molecular fraction drops sharply. Thus the cold gas is mostly confined to the spiral arms, and the gas is warmed in the interarm regions. Dobbs et al. (2008) found that roughly 62 per cent of the H I was in the cold phase, where $T \leqslant 150$ K was their criterion for cold gas.

The shock region itself is much smaller than the $\sim$ 100 pc region behind it where the physical state of the ISM undergoes these interesting changes. In the original SPH simulations, the smoothing length decreases greatly in high-density regions, dropping to values of about 5 to 6 pc to resolve regions where the density approaches 10^{-22} g cm^{-3} (Dobbs 2008), which is approximately the peak density achieved for the shocked H I shown in figure 10. SPH simulations typically require several smoothing lengths to capture a shock, and the shock width in any numerical model will be considerably greater than any realistic shock width (Price 2008).

5 DISCUSSION

5.1 Comparison with Observational Data

The synthetic datacubes we have produced correspond to the Second Galactic Quadrant, for which the best comparison set is the Canadian Galactic Plane Survey, part of the International Galactic Plane Survey (Taylor et al. 2003). We compare below the general characteristics and features observed in both the synthetic and real data. By the very fact that our SPH galaxy is *not* the Milky Way, no strong agreement is expected *a priori*. The main purpose of the synthetic models is to investigate whether the geometry, kinematics, chemistry and thermodynamics of a spiral shock can produce HISA, as has been observed in the Perseus Arm of our Galaxy. In comparing the two datasets, we can discern what characteristics this relatively simple galaxy model has in common with Galactic H I observations.

In figure 11 we show the Galactic analogue of the synthetic H I channel map for region GHI that was shown in figure 3. The main difference observed across the Second Quadrant is the apparent confinement of H I gas to the plane in our synthetic data cubes, compared to the widespread and more diffuse distribution of atomic gas seen in the CGPS

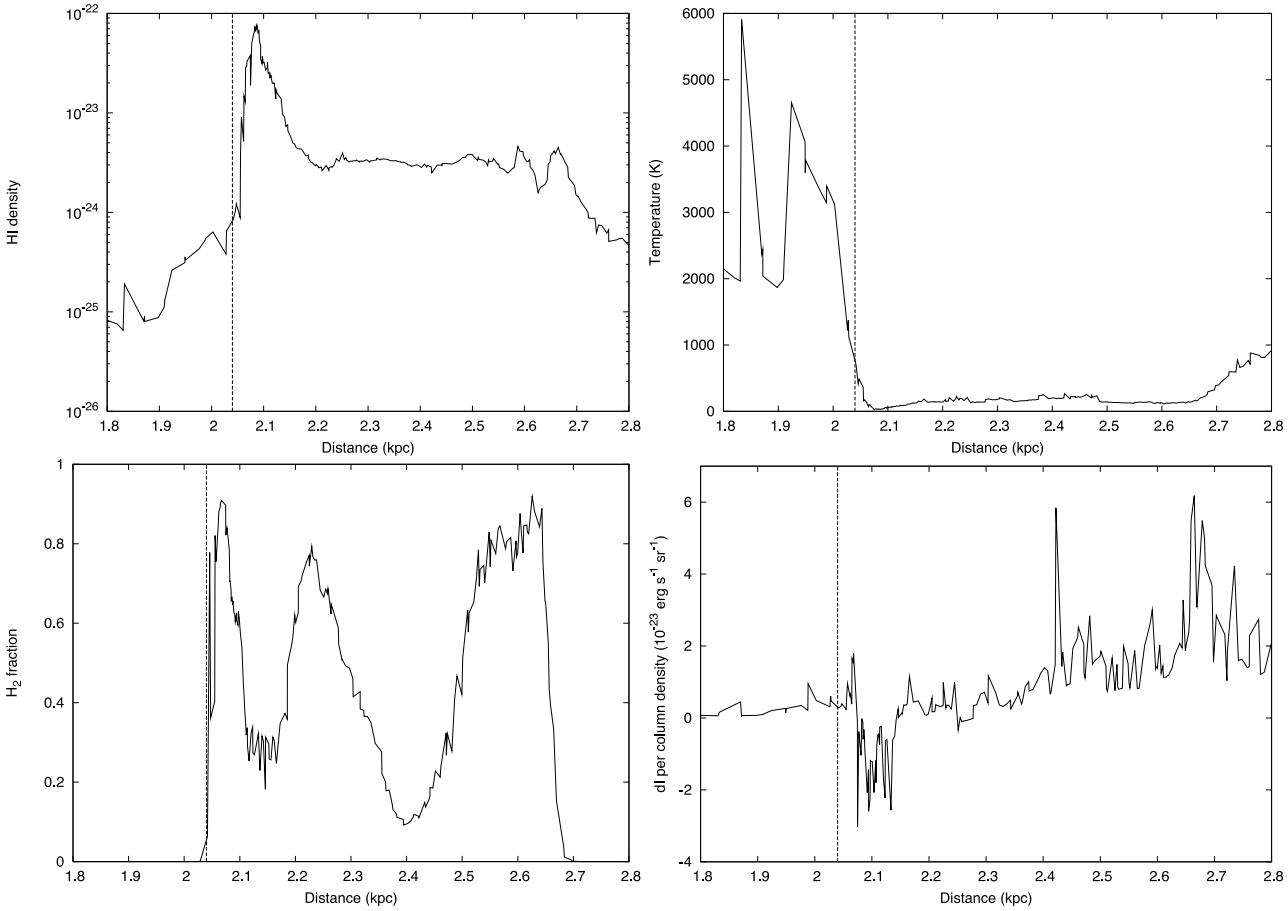

Figure 10. A close-up of the shock region seen in figure 8. The shock front position is approximated by the vertical dashed line. As H I density increases (top left) and temperature decreases (top right) , H_2 is formed in the shock region (bottom left), and background H I emission is absorbed (negative dI values in bottom right panel).

data. This is not surprising, given the lack of feedback mechanisms in the simulations that would serve to stir up the interstellar medium more vigourously—we will discuss this point further below. For now, we consider the consequences of this scale-height mismatch. For one, with a greater column density of H I toward the overdense midplane, the brightness temperatures for the synthetic line profiles are larger than what is observed in the Milky Way. Within the CGPS data brightness temperatures above 150 K are not common, yet in the synthetic cubes we encounter many regions with $T_b > 200$ K.

Unlike the scale height differences observed in the channel maps, the spiral structure in the SPH galaxy and the Milky Way show good agreement, in terms of the Perseus Arm, the main feature in the Second Quadrant of the Outer Galaxy. Figure 12 shows the Milky Way's mid-Second Quadrant midplane longitude-velocity distribution, which portrays a similar separation, on the order of $\Delta v_r \sim 40$ km s^{-1}, between local and Perseus Arm gas to that observed in figure 6. The presence of gas beyond the Perseus Arm is a main difference exhibited by the real data, as well as distinct H I features in the interarm gas. Additionally, the overall velocity width of the Galaxy's spiral arms is in general greater than that of the simulated galaxy. In the SPH galaxy, particles were given circular velocities with a velocity dispersion assigned to be $\sigma = 6$ km s^{-1}, while values of $\sigma \sim 8$ km s^{-1} or greater typically describe the H I of our Outer Galaxy (Saha et al. 2009). Many factors contribute to such a dispersion value, including feedback mechanisms and a warped disk; Dobbs & Price (2008) also found that magnetic fields broaden spiral arms in SPH galaxy simulations.

5.2 The Role of Feedback

The interstellar medium of our Galaxy is constantly disrupted, by both external and internal agents. The inflow of gas from satellite galaxies and high-velocity clouds provides fuel for future generations of molecular clouds and stellar systems. Numerous feedback processes from stellar evolution also add energy and momentum to the ISM from within: outflows, supernova shocks and winds from individual stars or stellar associations. With these agents absent from the simulated galaxy, our synthetic observations correspond to a rather quiescent version of a Milky Way-type galaxy. The consequences are abundantly clear in our synthetic datacubes. H I clouds collect toward the midplane and cool, with nothing to destroy them, resulting in larger than expected column and number densities. Thus the lower scale height seen in our simulated galaxy is well explained. If our synthetic data had shown agreement with the H I scale

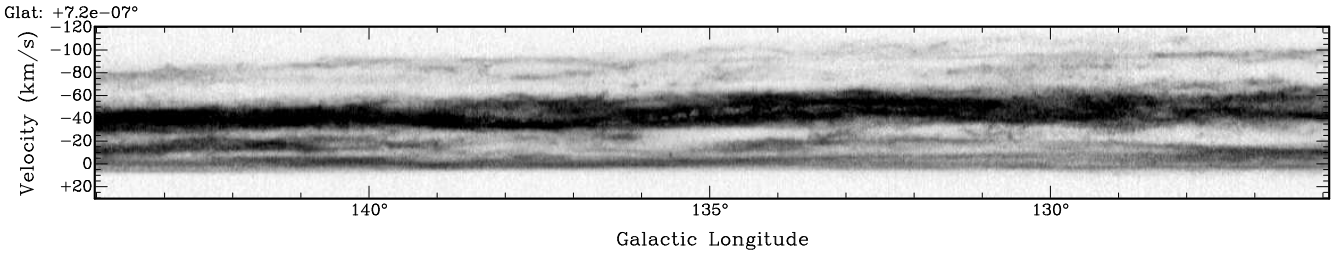

Figure 12. Longitude-velocity diagram of Milky Way H I emission near $\ell = 135°, b = 0°$ as observed with CGPS data.

height suggested by the CGPS data, then the importance of feedback in contributing to the overall structure of the ISM would be severely diminished.

Much of the H I distribution in our Galaxy can be described with words such as filaments, shells, and bubbles. Interstellar bubbles are created by outward forces originating from a central nidus. Shells and filaments form as a result of bubbles encountering each other, or other ISM structures, and their evolution is also aided by radiative and magnetic field effects. Without the injection of supernova-like events or winds from OB associations, the simulated galaxy cannot be expected to recreate the filamentary structure observed with H I observations of the Milky Way. Hence feedback is a possible solution to both the overconfinement of H I in the midplane, as well as the non-filamentary nature of the H I channel maps. Feedback should also increase the velocity dispersion of the simulated galaxy's spiral arms, since the mixing of the H I will certainly result in gas with a wider range of radial velocities.

5.3 Future Work

The simulation used in this paper provides a basis with which to compare future simulations which include more physical processes. As highlighted above, feedback appears to be instrumental in reproducing the correct structure (holes, filaments) and vertical distribution of the ISM. Moreover, magnetic fields are an important source of pressure, supporting the gas in the vertical direction (Cox 2005). In addition, magnetic fields are likely to reduce thermal instability in the gas (Field 1965; Hennebelle & Pérault 2000; Heitsch et al. 2009), which could reduce the amount of HISA seen in our simulated observations. On the other hand, self gravity will promote the formation of dense H I or molecular structures in the midplane, particularly at higher surface densities. Our synthetic observations of the H I distribution and the resulting HISA properties in these future simulations will demonstrate the cumulative effect of the added physics.

As the molecular fraction of the SPH galaxy evolves, formation of H_2 and CO take place using prescribed rate equations (Dobbs et al. 2008). The simplicity of the two-level hyperfine 21-cm transition makes the production of the synthetic H I spectra rather straightforward, compared to the detailed balance calculations required for other ISM tracers. Still, in principle the TORUS code can be adapted to produce synthetic observations of any species present in the original simulation. Rundle et al. (2010) have achieved synthetic molecular line observations for several species, including CO, for far-field view simulated observations of molecular clouds with TORUS. We will integrate their work to produce a synthetic CO galactic plane survey to complement our H I data. Besides spectral lines, we will also aim to produce realistic maps of continuum emission from dust.

The use of numerical simulations also offers the unique opportunity to trace individual features in the time domain. The simulation we used here from Dobbs et al. (2008) and others like it show the evolution of atomic hydrogen clouds as they encounter shocks in spiral arms, form molecular clouds, and eventually disperse as they exit the spiral arm on the other side. Radio observations can only piece together this scenario by observing multiple clouds at different stages of this evolution. In a future study we will recreate our synthetic Galactic Plane survey for several timesteps of a numerical solution, and track the evolution of the H I profiles of gas clouds which pass through spiral shocks.

In all of the above studies, we can also extend our synthetic Galactic Plane survey to other parts of the simulated Galaxy. From our chosen observer position, only lines of sight within $|\ell| < 46°$ are affected by the absence in the model domain of the inner 5 kpc of the galaxy. Thus we can extend our investigation to include H I observations from other components of the IGPS for comparison.

6 SUMMARY

We have demonstrated our ability to conduct a synthetic Galactic Plane H I survey. With the aid of the versatile TORUS code, we converted an SPH simulation of a spiral galaxy section into a set of H I datacubes predicting the brightness temperature distribution from an observer's position within that galaxy. With these cubes we can trace global features such as HISA and spiral arm structure, and in comparison with Galactic Plane Survey cubes of our Galaxy, we find common features, as well as clear and explicable differences in the H I distribution. The main differences seen, which include a lack of filamentary structure, a lower H I disc scale height, and spiral arms with a lower velocity dispersion, may be well explained by the absence of feedback processes that would conspire to mix the SPH galaxy's ISM more vigourously. We have shown that HISA is produced naturally by the influence of a spiral arm in the outer galaxy, where little or no HISA would otherwise be expected, because the unperturbed line-of-sight velocity field is monotonic with distance. With future SPH simulations that in-

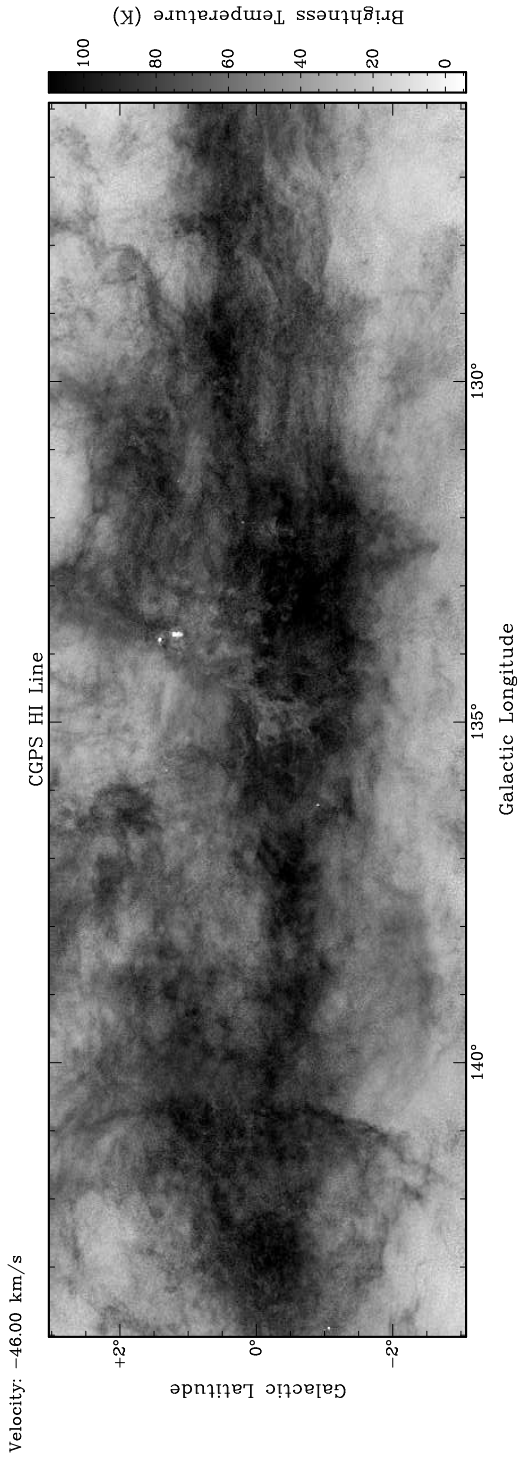

Figure 11. CGPS Channel map of Perseus Arm gas centered on $\ell = 135°$, $b = 0°$.

clude feedback mechanisms, we will discern whether stellar processing of interstellar gas leads to a closer match between the model and actual galaxy. We will also track the evolutionary trajectory of atomic clouds seen as HISA, to investigate further the early stage of molecular cloud formation.

ACKNOWLEDGMENTS

We wish to thank the referee for making excellent suggestions which aided greatly in the presentation of this work. The research leading to these results has received funding from the European Community's Seventh Framework Programme under grant agreement n° PIIF-GA-2008-221289. C.L.D.'s research at Exeter was conducted as part of the award "The formation of stars and planets: Radiation hydrodynamical and magnetohydrodynamical simulations," made under the European Heads of Research Councils and European Science Foundation EURYI (European Young Investigator) Awards scheme, and supported by funds from the Participating Organisations of EURYI and the EC Sixth Framework Programme. Calculations with TORUS were performed using the University of Exeter Supercomputer. The research presented in this paper has used data from the Canadian Galactic Plane Survey, a Canadian project with international partners supported by the Natural Sciences and Engineering Research Council.

REFERENCES

Acreman, D. M., Douglas, K. A., Dobbs, C., & Brunt, C. 2010, submitted (Paper I)
Bergin, E. A., Hartmann, L. W., Raymond, J. C., & Ballesteros-Paderes, J. 2004, ApJ, 612, 921
Cox, D. P. 2005, ARA&A, 43, 337
Dixon, W. V. D., Hurwitz, M., & Bowyer, S. 1998, ApJ, 492, 569
Dobbs, C. L. 2008 MNRAS, 391, 844
Dobbs, C. L., Glover, S. C. O., Clark, P. C., & Klessen, R. S. 2008 MNRAS, 389, 1097
Dobbs, C. L., & Bonnell, I. 2007, MNRAS, 376, 1747
Dobbs, C. L., & Price, D. J. 2008, MNRAS, 383, 497
Douglas, K. A., & Taylor, A. R. 2007, ApJ, 659, 426
Field, G. B. 1965, ApJ, 142, 531
Gibson, S. J., Taylor, A. R., Higgs, L. A., Brunt, C. M., & Dewdney, P. E. 2005, ApJ, 626, 195
Gibson, S. J. 2006, BAAS, 38, 124
Goldsmith, P. F., Li, D., & Krčo, M. 2007, ApJ, 654, 273
Harries, T. J. 2000, MNRAS, 315, 722
Heitsch, F., Stone, J. M, & Hartmann, L. W. 2009, ApJ, 695, 248
Hennebelle, P. & Pérault, M. 2000, A&A, 359, 1124
Kavars, D. W., Dickey, J. M., McClure-Griffiths, N. M., Gaensler, B. M., & Green, A. J. 2005, ApJ, 626, 887
Kavars, D. W. 2006, PhD Thesis, U. Minnesota
Kerp, J., Winkel, B, & Kalberla, P. M. W. 2009, arXiv: 0910.1421
Klaassen, P. D., Plume, R., Gibson, S. J., Taylor, A. R., & Brunt, C. M. 2005, ApJ, 631, 1001
Li, D., & Goldsmtih, P. F. 2003, ApJ, 585, 823
McClure-Griffiths, N. M., Dickey, J. M., Gaensler, B. M., Green, A. J., Haverkorn, M, & Strasser, S. 2005, ApJS, 158, 178
McClure-Griffiths, N. M., Dickey, J. M., Gaensler, B. M., Green, A. J., & Haverkorn, M. 2006, 652, 1339
McClure-Griffiths, N. M., Pisano, D. J., Calabretta, M. R., Ford, H., Lockman, F. J., Stavely-Smith, L., Kalberla, P. M. W., Bailin, J., et al. 2009, ApJS, 181, 398

Magnani, L. & Siskind, L. 1990, ApJ, 359, 355
Oka, T., Kamegai, K., Hayashida, M., Nagai, M., Ikeda, M., Kuboi, N., Tanaka, K., Bronfman, L., & Yamamoto, S. 2005, ApJ, 623, 889
Oort, J. H.,Kerr, F. J., & Westerhout. G. 1958, MNRAS, 118, 379
Peek, J. E. G., Stanimirovic, S., Putman, M. E., Heiles, C., Douglas, K. A., Korpela, E. J., & Gibson, S. J. 2008, in *Mapping the Galaxy and Nearby Galaxies*, ASSP Conference Proceedings, 324
Peek, J. E. G., Heiles, C., Putman, M. E., & Douglas, K. 2009, ApJ, 692, 827
Pelupessy, F. I., & Papadopoulos, P. P. 2009, ApJ, 707, 954
Price, D. J. 2008, JCoPh, 227, 10040
Putman, M. E., Peek, J. E. G., Muratov, A., Gnedin, O. Y., Hsu, W., Douglas, K. A., Heiles, C., Stanimirovic, S., et al. 2009, ApJ, 703, 1486
Roberts, W. W. 1972 ApJ, 173, 259
Rundle, D. A., Harries, T. J., Acreman, D. A., & Bate, M. R. 2010, submitted
Saha, K., Levine, E. S., Jog, C. J., & Blitz, L. 2009, 697, 2015
Stil, J. M., Taylor, A. R., Dickey, J. M., Kavars, D. W., Martin, P. G., Rothwell, T. A., Boothroyd, A. I., Lockman, F. J., & McClure-Griffiths, N. M. 2006, AJ, 132, 1158
Taylor, A. R., Gibson, S. J., Peracaula, M., Martin, P. G., Landecker, T. L., Brunt, C. M., Dewdney, P. E., Dougherty, S. M., et al. 2003, AJ, 125, 3145
van Loon, J. Th., Stanimiorivc, S., Putman, M. E., Peek, J. E. G., Gibson, S. J., Douglas, K. A., & Korpela, E. J. 2009 MNRAS, 396, 1096
Wannier, P. G., Andersson, B.-G., Federman, S. R., Lewis, B. M., Viala, Y. P., & Shaya, E. 1993, ApJ, 407, 163

This paper has been typeset from a TEX/ LATEX file prepared by the author.